Evaluation of N2 and CO2 pyrolyzed biochars in remediation studies: Adsorption and immobilization of potentially toxic elements in water and contaminated soil, and the impact

Chemical Engineering Science 324 (2026) 123315

Contents lists available at ScienceDirect

Chemical Engineering Science

journal homepage: www.elsevier.com/locate/ces

Evaluation of N_2 and CO_2 pyrolyzed biochars in remediation studies: Adsorption and immobilization of potentially toxic elements in water and contaminated soil, and the impact on soil properties

Premchand Premchand [a,d,e], Francesca Demichelis [a,*], Elio Padoan [b], Faten Khelifi [b], David Chiaramonti [c], Samir Bensaid [a], Debora Fino [a]

[a] Department of Applied Science and Technology, Politecnico di Torino, Corso Duca Degli Abruzzi 24, 10129 Turin, TO, Italy
[b] Department of Agricultural, Forest and Food Sciences (DISAFA), University of Torino, Grugliasco, TO 10095, Italy
[c] Department of Energy, Politecnico di Torino, Corso Duca Degli Abruzzi 24, 10129 Turin, TO, Italy
[d] Department of Science, Technology and Society, University School for Advanced Studies IUSS Pavia 27100 Pavia, PV, Italy
[e] Swedish University of Agricultural Sciences, Department of Forest Biomaterials and Technology. 90183 Umea, Sweden

ARTICLE INFO

Keywords:
Rice husk
Pyrolysis
CO_2 atmosphere
Biochar
Heavy metals adsorption
Soil remediation
Metals immobilization

ABSTRACT

Using CO_2 medium (instead of inert gas) during pyrolysis has been reported to improve biochar properties, particularly textural and surface properties; however, its investigation in remediation applications has received little attention. In this study, biochar prepared from rice husk pyrolysis under CO_2 atmosphere (BCC) and under N_2 atmosphere (BCN) was investigated for efficacy in removing zinc (Zn^{2+}) and lead (Pb^{2+}) in water, immobilizing potentially toxic elements (PTE) in soil, and improving physicochemical properties of a mining soil. Results showed that for aqueous metals adsorption, both biochars followed the pseudo-second order kinetic model. BCC exhibited greater Zn^{2+} adsorption capacity and efficiency (26 mg/g, 52 %) compared to BCN (22 mg/g, 45 %). In contrast, both biochars had comparable Pb^{2+} adsorption efficiency (40 %). Furthermore, five-week biochar-soil incubation experiments revealed that, compared to control soil, both biochars significantly improved soil physicochemical properties, such as increasing total and organic carbons, pH, water holding capacity, and cation exchange capacity as the dose increased from 3 to 10 %. However, both biochars showed statistically insignificant differences at similar doses, revealing that soil improvements were strongly dose-dependent rather than biochar type. PTE immobilization experiments revealed that both biochars numerically reduced the bioavailability of all PTEs (Zn, Pb, Cr, Cu, Cd, Ni, Mn) in soil, but the difference was not statistically significant under the tested conditions.

1. Introduction

Rapid industrial and agricultural development due to population growth has led to an abundance of potentially toxic elements (PTE) in water and soil sources, posing a major risk to public health and environmental ecosystems (Wang et al., 2022b; Yu et al., 2025).

Mining activities are one of the primary sources of these PTE. Due to their non-biodegradable nature, PTEs can persist in soil and water for long periods if not properly managed (Padoan et al., 2020), negatively impacting soil fertility and key physicochemical properties such as pH, cation exchange capacity (CEC), electrical conductivity (EC), and nutrient contents (Penido et al., 2019). Therefore, it is crucial to develop soil remediation strategies to restore mining affected areas where elevated concentrations of PTE are present (Lu et al., 2018) and attention should be given on sustainable and environmentally friendly techniques to achieve the carbon neutrality (Li et al., 2025). Currently, many remediation techniques have been used to restore soil in mining areas, including chemical immobilization, phytoremediation, bioremediation, and physical remediation (Gao et al., 2022; Xiong et al., 2023). Among these, metal's immobilization through the addition of organic amendments such as biochar is a relatively new remediation technique and has been extensively researched recently (Jin et al., 2016).

Biochar, a carbonaceous char produced from biomass through a thermochemical process, has been considered as an effective

* Corresponding author.
E-mail address: francesca.demichelis@polito.it (F. Demichelis).

https://doi.org/10.1016/j.ces.2026.123315
Received 25 August 2025; Received in revised form 30 December 2025; Accepted 4 January 2026
Available online 5 January 2026

amendment to improve the physicochemical characteristics of soil as well as to reclaim metals contaminated soil and water (Zhao et al., 2020). Biochar in soil or water can absorb or immobilize PTE through various mechanisms, including physical adsorption, electrostatic interaction, complexation, ion exchange, and precipitation, either alone or in combination (Gao et al., 2022). Furthermore, biochar is widely regarded as an effective soil amendment material for improving soil health and productivity, particularly in heavily weathered soil. Biochar amendment with soil has been shown to regulate soil pH, reduce soil bulk density while increasing CEC, organic carbon, porosity, adsorption capacity, water holding capacity (WHC), and nutrient content (Liu et al., 2018a; Zhang et al., 2021).

Nevertheless, the efficiency of biochar in remediation applications primarily depends on its properties (specific surface area, porosity, carbon content, functional groups, cation exchange capacity, etc.), which are in turn determined by biochar production conditions (feedstock type, production temperature, heating rate, and pyrolysis atmosphere) (Chen et al., 2011; Premchand et al., 2024b). Among various biochar production technologies, slow pyrolysis under an inert atmosphere is regarded as promising because it maximizes biochar yield while retaining a stable and carbon-rich biochar (Yargicoglu et al., 2015). Still, as biochar use in many specific applications is limited by its low surface area, porosity, and minor functional groups, an effort has been made recently to improve its physicochemical properties using various modification strategies (Aktar et al., 2022; Nguyen et al., 2021). Among these, using CO_2 in pyrolysis instead of inert gas has recently gained attention and has been suggested as an effective way to improve biochar textural properties, which are extremely beneficial for remediation applications (Lee et al., 2017; Lu et al., 2018; Premchand et al., 2023a).

Using CO_2 in pyrolysis may provide economic and environmental benefits, such as improved biochar properties, pure inert gas replacement (Lee et al., 2017) as well as utilizing the problematic greenhouse gas to reduce climate effect (Fan et al., 2025). Despite considerable studies on the effect of CO_2 on biochar production and properties, little emphasis has been placed on its performance in practical applications. To the best of our knowledge, only a few studies investigated the effect CO_2 derived biochars in different applications, including its effect on biochar's nitrogen migration and distribution in the soil (Tan et al., 2018; Ye et al., 2020), adsorption of copper and methylene blue (Cho et al., 2016), and arsenic (Cho et al., 2017).

Therefore, the current study comprehensively investigates the effect of biochars previously produced from rice husk biomass under N_2 and CO_2 atmospheres (Premchand et al., 2023b; Premchand et al., 2024a), on the adsorption of zinc (Zn^{2+}) and lead (Pb^{2+}) in solution and on the effect of their addition to contaminated mining soil, both on the physicochemical properties and on the bioavailability of the contaminants (PTE). This study contributes to the systematic simultaneous investigation of the performance evaluation of CO_2 biochar in both aquatic and contaminated soil environments on a wide range of PTEs to find its potential applications in environmental remediation techniques.

2. Materials and methods

2.1. Biochar

The rice husk (RH) feedstock was used for biochar preparation and was provided by Ecopack, Piobesi, Italy, and was used as received. The rice husk was chosen because of the massive production and consumption of rice worldwide, which generates an abundance of rice husks as waste and has a huge potential for conversion into biochar (Jahan et al., 2024).

The characterization analysis methods (proximate, elemental, and thermogravimetric analysis) of the rice husks are presented in Supplementary Materials in Table S1 and Fig. S1 and explained in detail in Text S1.

The biochar was produced through slow pyrolysis in a fixed-bed pyrolysis reactor with an electric heater and two thermocouples installed at different levels within the reactor, as shown in Fig. 1.

Before heating, the reactor was manually filled with 10 g of RH feedstock, purged with CO_2 or N_2, and heated with a 15 °C/min heating rate to 600 °C with a residence time of 1 h. These parameters were chosen from an earlier study demonstrating better biochar properties under these conditions (Premchand et al., 2023b). Following the pyrolysis process, the reactor was left to cool to room temperature before the biochar was manually collected, weighed, and stored for characterization analyses. Each experiment was replicated three times to ensure reproducibility.

2.2. Soil

A mine-affected soil has been sampled in the Gorno mining basin, located about 25 km northeast of Bergamo in the Orobian Alps (Lombardia Region, Italy). Its main mineralization was sphalerite (ZnS) and galena (PbS) with traces of chalcopyrite ($CuFeS_2$), pyrite and marcasite (FeS_2), and argentite (Ag_2S), respectively (Mehta et al., 2020). The soil has been chosen among the ones used in a previous study (Padoan et al., 2020). In brief, a composite soil sample was collected at a depth of 0–15 cm by combining five subsamples, each taken from the center and vertices of a 2-by-2-meter square to ensure consistency and take a representative sample of the whole area. The sample was then air-dried, sieved to 2 mm, and characterized as in (Padoan et al., 2020).

2.3. Zinc and lead adsorption experiments

For the aqueous metals' adsorption experiments, zinc (Zn^{2+}) and lead (Pb^{2+}) were chosen due to their toxicity and abundance in the studied soil. The solutions of 100 mg/L of Zn^{2+} or Pb^{2+} were prepared by dissolving zinc nitrate hexahydrate ($Zn(NO_3)_2{\cdot}6H_2O$) or lead(II) nitrate ($Pb(NO_3)_2$) in ultrapure Milli-Q® water. Both chemicals were bought from Sigma-Aldrich with > 99.5 % purity. All the adsorption experiments were performed at pH 6.5 (Alam et al., 2018) with a biochar dose of 2 g/L to avoid metal precipitation, since the aim of the study was to investigate the adsorption of free metals, rather than precipitation. The initial and final metal concentrations in solutions were determined using inductively coupled plasma emission spectroscopy (ICP- OES, iCAP PRO Thermo Fisher) after filtering through a membrane filter (0.45 μm). The adsorption capacity (Q_t) and adsorption efficiency (removal %) were calculated using Eqs. (1) and (2), adopted from the literature (Li et al., 2020; Premchand et al., 2025).

$$\mathrm{Qt} = \frac{(C_0 - C_t) \times V}{m} \tag{1}$$

$$\mathrm{Removal\%} = \frac{(C_0 - C_t)}{C_0} \times 100 \tag{2}$$

where Q_t is the adsorption capacity in mg/g, C_o and C_t are the initial and final metal concentrations in mg/L, V is the solution volume (L), and m is the adsorbent (biochar) mass in g, respectively.

For the adsorption kinetics, 1.0 g of biochar was added to 500 mL of Zn^{2+} or Pb^{2+} solutions with a 100 mg/L concentration and stirred at 180 rpm at room temperature. The samples were collected at 10, 30, 60, 120, 240, 360, 480 min and after 24 h.

To evaluate the adsorption process and mechanics insights, the experimental data were fitted using commonly used kinetic models, including Pseudo-first order (PFO), Pseudo-second order (PSO), Intraparticle diffusion (IDP), and Elovich kinetic models (Abdelhafez and Li, 2016; Kılıç et al., 2013). Each model describes distinct adsorption mechanisms, i.e. PFO assumes the physisorption, or surface interaction, whereas PSO represents chemisorption as the main adsorption driving mechanism, and both are frequently applied to heterogeneous sorbents

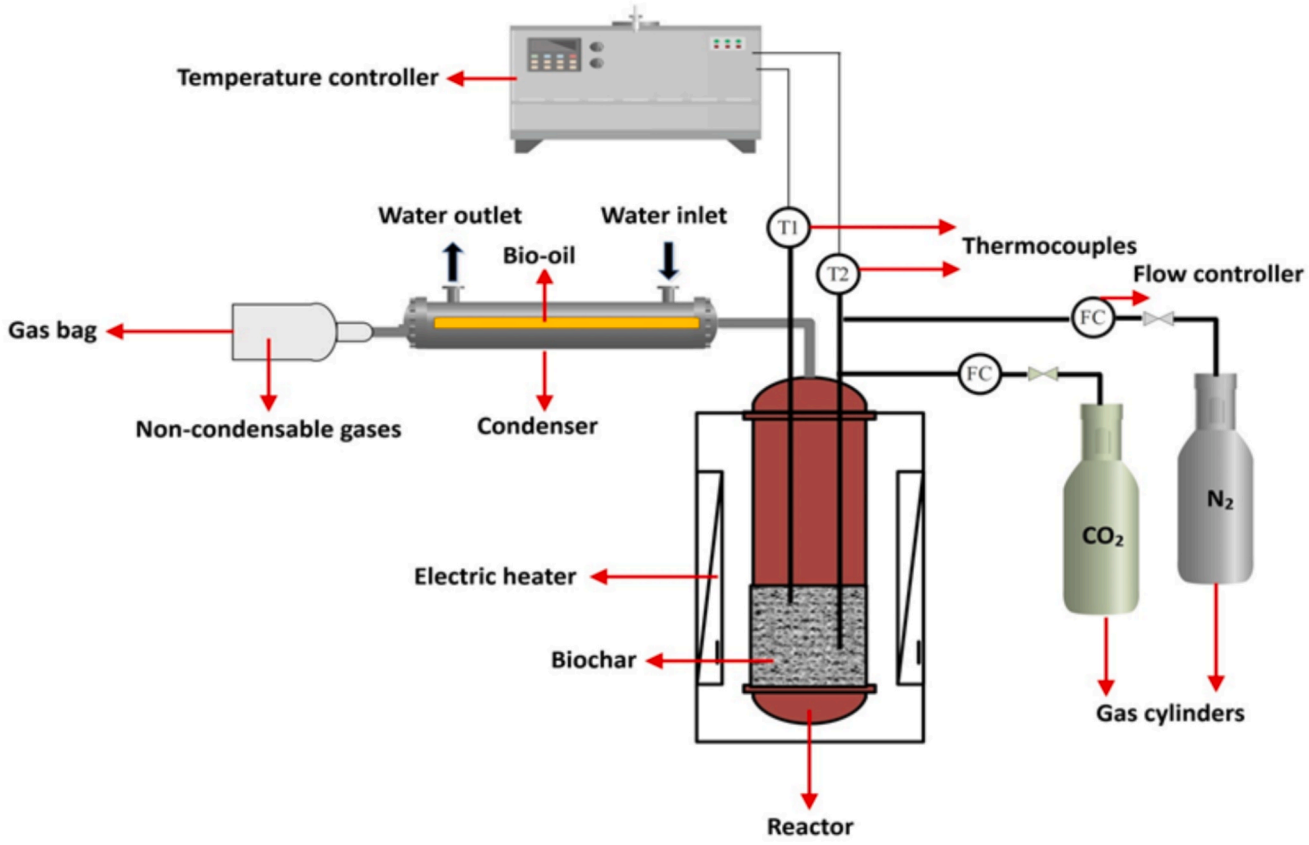

Fig. 1. Schematic illustration of pyrolysis reactor setup (Premchand et al., 2023b).

like biochar (Chen et al., 2011; Kołodyńska et al., 2012). Furthermore, the IDP model assumes adsorption by pore diffusion and surface adsorption, while the Elovich model was applied to better evaluate the chemical adsorption, which depicts the heterogeneous diffusion process regulated by reaction rate and diffusion factor (Kołodyńska et al., 2012; Qiao et al., 2021). The linear and non-linear mathematical equations for the studied kinetics are presented in Table 1, adopted from previous studies (Kılıç et al., 2013; Mele et al., 2024).

2.4. Biochar-soil incubation experiments

To investigate the effect of biochar amendment on metal immobilization and soil physicochemical properties, different doses (0 %, 3 %, 5 %, and 10 %) of both biochars (BCN and BCC) were thoroughly mixed with soil (50 g) and placed in 500 mL polyethylene bottles with a lid and incubated at 25 ± 1 °C in the dark for 5 weeks to investigate the effect of lower medium and higher biochar doses (Kumar et al., 2013). The soil's moisture content was set at 80 % of its water-holding capacity and maintained throughout the incubation period by regularly weighing the bottles, checking for weight losses, and correcting the weight by adding the appropriate deionized water. Three replicates were kept for each treatment, including control soil (CS), 3 % biochar dose of BCN (3-BCN) and BCC (3-BCC), 5 % biochar dose of BCN (5-BCN) and BCC (5-BCC), and 10 % biochar dose of BCN (10-BCN) and BCC (10-BCC), respectively. Following the incubation period, the samples were air-dried for physicochemical analysis, as described in section 2.5.

Table 1
Summary of the adsorption kinetics models used in this study.

Kinetic model	Linear	Non-linear
Pseudo-First Order	$\ln(q_e - q_t) = \ln q_e - k_1 t$	$q_t = q_e(1 - e^{k_1 t})$
Pseudo-Second Order	$\frac{t}{q_t} = \frac{1}{k_2 q_e^2} + \frac{1}{q_e}$	$q_t = \frac{k_2 q_e^2 t}{1 + k_2 q_e t}$
Intra-Particle Diffusion	$q_t = K_{diff}.t^{0.5} + C$	$q_t = K_{diff}.t^{0.5} + C$
Elovich	$q_t = \frac{1}{\beta} ln(t) + \frac{1}{\beta} ln(\alpha\beta)$	$q_t = \frac{1}{\beta} ln(\alpha\beta) + \frac{1}{\beta} ln(t)$

Where, q_e and q_t represent the adsorption capacities (mg.g^{-1}) at equilibrium and given time (t), k_1 (h^{-1}), k_2 (g·mg^{-1}·min^{-1}), and K_{diff} (mg. g^{-1}. min$^{-0.5}$) are the adsorption rate constants, C is the intercept, α is initial adsorption rate (mg. g^{-1}·min^{-1}) and β is the desorption constant (g.mg^{-1}).

2.5. Characterization analyses of biochar and soil

Biochar has been characterized as follows: the specific surface area and pore volume analysis were carried out on the Micromeritics TriStar II 3020 using N_2 adsorption–desorption isotherms at −196 °C in liquid nitrogen by degassing samples in a vacuum for 2 h at 300 °C. The elemental (C, H, N, and S) analysis of biochar was performed using an elemental analyzer (UNICUBE, Elementar Analyses System GmbH, Germany), and an Energy-Dispersive Spectroscopy (EDS) analysis was performed on a Field Emission Scanning Electron Microscope (Zeiss Merlin) equipped with an EDS detector. The surface functional groups of biochar were examined using the F-TIR Spectrophotometer (Bruker Equinox 55) on ATR mode.

The pH and electrical conductivity (EC) of the biochar were measured potentiometrically using a 1:20 biochar/water ratio (Premchand et al., 2024a). The point of zero charge (pH_{PZC}) of biochar was determined using the salt addition method (Nguyen et al., 2021). First, ten glass flasks were filled with 20 mL of 0.1 M NaCl solution, and the pH of each solution was adjusted to 3, 4, 5, 6, 7, 8, 9, 10, 11, and 12 with 0.1 M HCl or NaOH. Then, 0.2 g of biochar was mixed with each solution, shaken for 24 h, filtered, and the solution's final pH was measured. A graph was plotted between ΔpH ($pH_{final} - pH_{initial}$) and initial pH, and pH_{PZC} was determined at the intersection point.

The water holding capacity (WHC) of biochar was determined according to the previous studies (Mao et al., 2019; Yargicoglu et al., 2015). First, a known amount of air-dried biochar sample (5.0 g) was placed on dried Whatman grade 5 filter paper (2 μm) attached to a glass funnel placed over the flask. Then, 50 mL of deionized water was slowly poured into the biochar until completely saturated, and it was allowed to drain gravimetrically for 1 h at room temperature. The WHC was then determined as the ratio of water retained by the biochar alone to the mass of dry biochar after accounting for the water absorbed by the filter paper.

Soil has been characterized as follows. The particle size of the soil was measured by the sieve and pipette method (Padoan et al., 2020). The soil's pH and EC were determined potentiometrically at a ratio of 1:2.5 (soil to water) after two hours of shaking (Zhong et al., 2025) and total C, N, S and H contents in soil were determined via dry combustion and the volumetric method was used to measure soil carbonates using 1.0 g of soil and 10 mL of HCl and measuring the amount of CO_2 in a closed system (Padoan et al., 2021). For quality assurance, samples were digested in duplicates with an analytical blank and an internal laboratory standard (Agricultural soil of Piedmont-Italy) and a certified reference material (CRM141R Community Bureau of Reference, Geel, Belgium) against which the results were checked. The average recovery for the elements studied in all batches of analysis was between 95 % and 107 %. Before analysis and after a set of 10 samples, the instrument was calibrated with matrix-matched external standards. Organic carbon was calculated as the difference between total carbon (measured by an elemental analyzer) and carbonates. The WHC of soil was measured using the same method as described above for biochar. The cation exchange capacity (CEC) of soil was determined using the barium chloride method (Rhoades, 1982). Briefly, 2.0 g of soil was saturated with a 0.1 M $BaCl_2$ solution, rinsed with deionized water, and barium ions were exchanged with 0.1 M $MgSO_4$. The barium ions were then measured using 0.05 N ethylenediaminetetraacetic acid (EDTA) titration in a pH 10 buffer solution using an indicator. The CEC was calculated using the EDTA volume required for titration. The total metal content (pseudo-total) in soil was determined using *aqua regia* (HCl/HNO_3, 3:1 v/v) extraction via sand bath digestion, and filtration followed by ICP-OES analysis (Padoan et al., 2020). The bioavailable metal contents in soil were determined using the diethylenetriaminepentaacetic acid (DTPA) extraction method, which involved adding 5 g of soil to a 10 mL solution of 5 mM DTPA and 10 mM $CaCl_2$ and shaking for 1 h before centrifugation and filtration through a Whatman 5 filter paper (Dai et al., 2004). The metal content was then determined using ICP-OES analysis.

2.6. Statistical analysis

The physicochemical properties of BCN and BCC were compared using independent two-sample t-tests (Welch's *t*-test) to determine the significant difference between the two biochars. Furthermore, a two-way ANOVA was used to investigate the main effects and interactions of biochar type and dosage level on soil properties and PTE immobilization. Statistical calculations were performed using OriginPro 2022, with a significance threshold of $p < 0.05$.

3. Results and discussion

3.1. Characteristics of biochars and soil

The physicochemical properties of biochar prepared under N_2 atmosphere (BCN) and CO_2 atmosphere (BCC), and soil are listed in Table 2 and discussed in detail in the subsequent subsections.

3.1.1. Biochar

Overall, compared to BCN, BCC exhibited slightly higher ash, pH ($p \geq 0.05$), pH_{PZC} ($p < 0.05$), electrical conductivity, and carbonates. This suggests that the oxidative nature of CO_2 may have facilitated the decomposition of organic materials, leaving behind more mineral residues, which in turn may have contributed to the higher pH and ash content (Premchand et al., 2023a, b; Premchand et al., 2024a). Moreover, during pyrolysis, the CO_2 atmosphere may have contributed to carbonates and other alkali salts formation, which raised alkalinity (Aktar et al., 2022). In elemental analysis, BCC had slightly more total carbon ($p < 0.05$) and nitrogen than BCN, indicating that CO_2 boosted the carbon enrichment by promoting the partial removal of volatile organic compounds while inhibiting the removal of nitrogenous compounds (Liu et al., 2018c).

Compared to BCN, BCC exhibited significantly ($p < 0.05$) higher specific surface area (141.0 m^2/g) and pore volume (0.08 cm^3/g) than BCN with a specific surface area of 55.7 m^2/g and pore volume of 0.02 cm^3/g. CO_2 has been considered to act as a physical activation agent at higher temperatures, which promotes the formation of micropores and mesopores, eventually enhancing the textural properties of the resultant biochars (Lee et al., 2017; Premchand et al., 2023a). The FT-IR analysis (Fig. S2) revealed that both biochars had similar functional groups; however, the intensities of the carbonyl (C=O), hydroxyl (O–H), and silicate groups (Si-O-Si) were slightly higher in BCC than in BCN which might be due to the oxidative effect of CO_2 (Lee et al., 2017; Premchand et al., 2023b). Furthermore, the water holding capacity (WHC) of BCC was 1.05 times higher ($p < 0.05$) than that of BCN, which could be attributed to increased pore volume and specific surface area, as well as slightly higher intensities of hydrophilic functional groups (C=O, O–H, C-O), which improved the BCC's water retention ability (Mao et al., 2019).

3.1.2. Soil

The physicochemical properties and total heavy metal content of the

Table 2
Physicochemical properties of biochars and soil (different letters indicate statistically significant differences between BCN and BCC using an independent two-sample *t*-test, and all values are reported as a mean ± standard deviation; n = 3).

Characteristic	BCN	BCC	Soil
pH	8.84 ± 0.03b	9.57 ± 0.07a	6.87 ± 0.03
pH_{PZC}	7.69 ± 0.91b	7.74 ± 0.16a	–
Ash (%)	33.5 ± 1.3a	34.4 ± 2.1a	–
C (%)	72.0 ± 2.14b	74.09 ± 2.08a	7.83 ± 0.25
H (%)	2.30 ± 0.11a	2.09 ± 0.13b	1.39 ± 0.04
N (%)	1.35 ± 0.07a	1.68 ± 0.18a	0.66 ± 0.03
S (%)	0.12 ± 0.001a	0.11 ± 0.002a	1.29 ± 0.44
*O (%)	24.23a	22.03b	88.93
C/N	53.3	44.1	11.9
O/C	0.34	0.30	–
Carbonates (%)	0.91 ± 0.05a	0.93 ± 0.01a	5.98 ± 0.62
Inorganic carbon (%)	0.10a	0.11a	0.72
*Organic carbon (%)	71.90a	73.98a	7.11
SSA (m^2/g)	55.7 ± 1.0b	141.0 ± 1.0a	–
Pore volume (cm^3/g)	0.02 ± 0.00b	0.08 ± 0.002a	–
WHC (g H_2O/g sample)	3.04 ± 0.02b	3.19 ± 0.01a	0.48 ± 0.11
EC (dS/m)	0.16 ± 0.02a	0.17 ± 0.01a	0.65 ± 0.07
CEC (meq/100 g)	–	–	22.6 ± 0.9
Clay (%)	–	–	6.0
Slit (%)	–	–	18.1
Sand (%)	–	–	75.9
Total metals (mg/kg)			
Fe			40642 ± 419
Mn			4380 ± 72
Zn			90712 ± 966
Cd			205 ± 10
Ni			28.0 ± 0.9
Cu			100 ± 2
Cr			62 ± 2
Pb			367 ± 3

Letters a and b represent significantly higher ($p < 0.05$, Welch's *t*-test).
* Calculated as a difference.

studied soil are shown in Table 2. The soil was sandy loamy, with a neutral pH (6.87) and 0.65 dS/m EC representing the salinity level of the soil (Tamiru et al., 2024). The soil contained a very high amount of carbon (7.83 %), due to its sampling position in a mountainous area and to the permanent grass covering. Mineralization was in balance, with C/N and C/H ratios of 11.9 and 5.6, respectively. The elemental analysis also revealed a high sulfur content (1.29 %) probably due to the input of mining debris, and the soil's electrical conductivity, cation exchange capacity, and water holding capacity were 0.65 dS/m, 22.6 meq/100 g, and 0.48 g H_2O/g soil.

The total concentrations of PTE in the soil were significantly high due to the sampling location and perhaps the addition of material during the past mining operations. Total concentrations of Zn, Mn, Pb, Cd, Cu, and Cr were 90712, 4380, 367, 205, 100, and 62 mg/kg, respectively, with Zn, Cd, and Pb^{2+} exceeding the limit set by Italian legislation for green and residential areas (Padoan et al., 2020). The presence of these metals can cause serious ecological issues for the entire eco system, including soil, water, and the general public, necessitating significant environmental attention (Asgari and Abdipour, 2025).

3.2. Biochar heavy metals (Zn^{2+} and Pb^{2+}) adsorption studies

3.2.1. Adsorption capacity and metals removal percentage

The adsorption capacity (mg/g) and adsorption efficiency (removal %) of Zn^{2+} and Pb^{2+} by BCN and BCC biochars until 600 min are shown in Fig. 2, while the adsorption behaviors until 24 h are shown in Fig. S4 (Supplementary materials).

As depicted in Fig. 2 (A), BCN Zn^{2+} adsorption capacity increased steadily over contact time, peaking at 22.45 mg/g at 24 h with an adsorption efficiency of 44.9 % (Fig. S4), indicating that BCN showed a moderate affinity for Zn^{2+} ions. The maximum Zn^{2+} ions were removed within the first 60 min, after which the adsorption rate slowed and

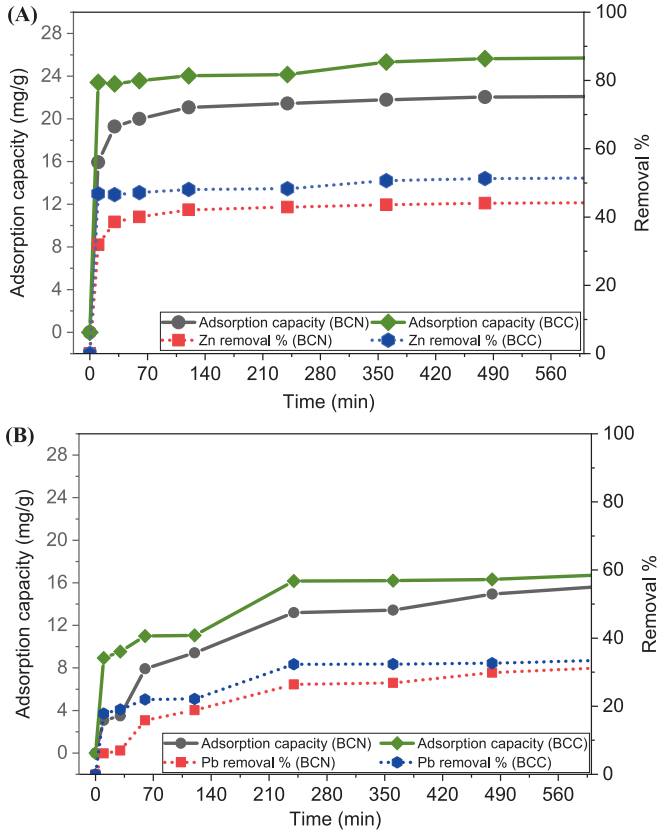

Fig. 2. Adsorption capacity and metals removal percentage for Zn^{2+} (A) and Pb^{2+} (B) by BCN and BCC biochars.

became constant after reaching 240 min, indicating that the surface adsorption sites were in equilibrium (Premchand et al., 2025). BCC, on the other hand, showed a significantly higher adsorption capacity, reaching 26.16 mg/g at 24 h (Fig. S4) with a removal efficiency of 52.3 %. BCC, like BCN, removed the most metal ions within the first 60 min, and the adsorption efficiency remained constant after about 360 min, indicating that BCC has a greater capacity for Zn^{2+} adsorption than BCN. The higher Zn^{2+} adsorption capacity of BCC over BCN can be ascribed to differences in physicochemical properties between the two biochars. BCC had an enhanced surface area and pore volume (Table 2), as well as oxygen functional groups, which may have improved the ion exchange of the BCC surface and complexation capacity by providing more active sites for Zn^{2+} adsorption (Van Hien et al., 2020; Zhao et al., 2020), which is consistent with its higher efficiency.

Looking at lead (Pb^{2+}) adsorption (Fig. 2 (B)), BCN adsorption capacity gradually increased with time, reaching a maximum of 20.12 mg/g with 40.3 % removal efficiency after 24 h (Fig. S4). In contrast to Zn^{2+}, Pb^{2+} adsorption appeared to be modest, particularly in the early stages (10–120 min), indicating a diffusion-limited process followed by a slower equilibrium phase. This could be due to the nature of lead ions and their interactions with the BCN surface, and in line with the previous study of Pb^{2+} adsorption by rice husk biochar (Shi et al., 2019). Similarly, BCC also exhibited a higher capacity and faster uptake (k_2 = 0.0011 $min^{-1}mg^{-1}$) for Pb^{2+} adsorption than BCN (k_2 = 0.0011 $min^{-1}mg^{-1}$) in the early and intermediate phases (up to 480 min), with a 32.6 % efficiency and an adsorption capacity of 16.31 mg/g. However, after 480 min, BCC's adsorption curve plateaued earlier and eventually became equal to BCN, reaching a maximum adsorption capacity of 19.38 mg/g and a removal efficiency of 38.8 % after 24 h. (Fig. S4).

Overall, for Zn^{2+}adsorption, BCC outperformed BCN at all time intervals, possibly due to its improved textural and structural properties. In contrast, Pb^{2+} adsorption behavior was time dependent; during the early and intermediate phases (up to 8 h), BCC outperformed BCN, but then BCN suppressed BCC. This suggests that lead adsorption is driven by a different mechanism than zinc adsorption, which appears to be influenced more by accessible porosity and total surface area. In contrast, lead adsorption may be primarily dependent on a small number of high-affinity sites (functional sites) that are found in both biochars. At the concentrations tested, the additional surface area provided by CO_2 biochar made a minimal contribution. In the previous studies, (Cho et al., 2016) compared the adsorption performance of CO_2 and N_2 biochars (produced from red seaweed) for methylene blue and copper and observed that the CO_2 modified biochar was more effective for methylene blue and less effective for copper removal despite having higher surface area and porosity than N_2 biochar highlighting the different mechanisms of action by both biochars.

3.2.2. Adsorption kinetics

The experimental data were analyzed using various kinetic models, including the pseudo-first order (PFO), pseudo-second order (PSO), intra-particle diffusion (IPD), and Elovich models. Figs. 3 and 4 compare the experimental and theoretical adsorption capacities of both biochars for both metals, while Table 3 presents the calculated kinetic parameters.

Concerning Zn^{2+} adsorption kinetics, as shown in Fig. 3, the PFO model did not fit well for both biochars because the theoretical adsorption capacity (equilibrium) values (4.50 mg/g BCN and 4.82 mg/g BCC) differed significantly from the experimental values (22.45 mg/g and 26.16 mg/g). The lower R^2 values (0.87 for BCN and 0.88 for BCC) demonstrated that the PFO model failed to adequately describe the adsorption process, implying that physisorption or surface interaction did not dominate the adsorption (Kołodyńska et al., 2012).

The PSO kinetic model demonstrated a strong agreement between theoretical and experimental adsorption data for BCN and BCC. The calculated adsorption capacity values (22.51 mg/g for BCN and 26.22 mg/g for BCC) closely matched the experimental values (22.45 mg/g

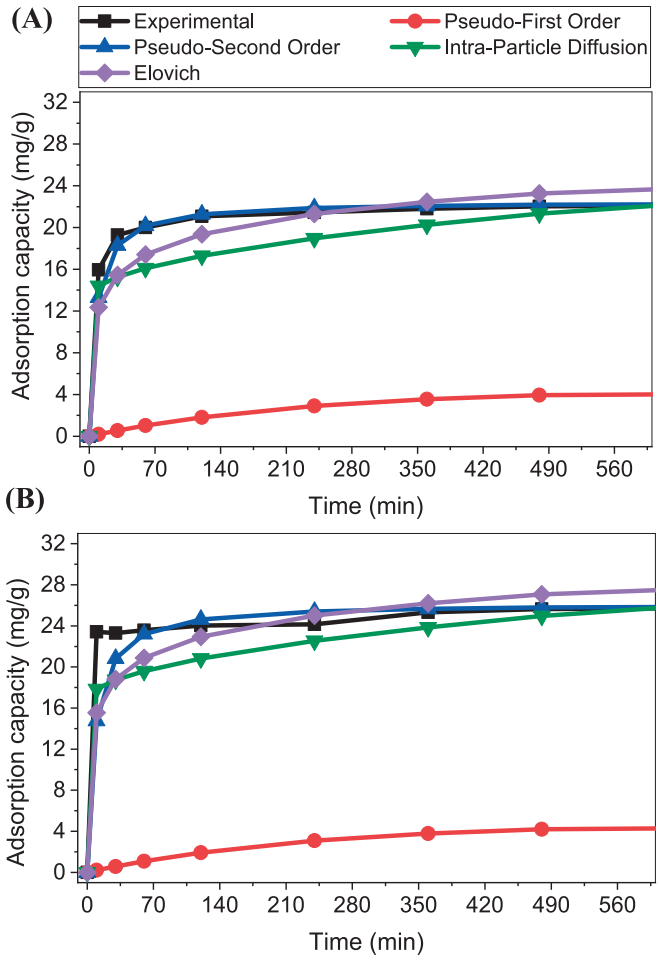

Fig. 3. Adsorption kinetics for zinc by BCN (A) and BCC (B) biochars (experimental and theoretical).

and 26.16 mg/g), indicating the accuracy of the PSO model. Furthermore, the correlation coefficients (R^2) for both biochars were 0.99, indicating that the adsorption process was chemically controlled and possibly involved electron-sharing or valence forces. The better fit suggests that chemisorption was the primary mechanism driving zinc adsorption in both biochars (Chen et al., 2011).

The IPD model showed multi-linearity, suggesting that adsorption took place in multiple stages, first as a fast surface adsorption stage and then as a slower diffusion stage into the pores of the biochar (Kołodyńska et al., 2012). BCC appeared to have faster diffusion kinetics, as evidenced by the slightly higher diffusion rate constant (K_{diff}) for BCC (0.38) than for BCN (0.37). The adsorption kinetics, however, cannot be explained by intra-particle diffusion alone, as indicated by the low R^2 values (0.28 for BCN and 0.19 for BCC).

Lastly, the Elovich kinetic model exhibited a reasonably well fit on the experimental data, as evidenced by correlation coefficient values of 0.75 for BCN and 0.71 for BCC, confirming that the chemisorption process dominated the zinc adsorption process. The Elovich parameters differed significantly between BCN and BCC, with BCC having a higher α value (55.18 $mg.g^{-1}{\cdot}min^{-1}$), indicating a higher initial adsorption rate than BCN with an α value of 22.67 $mg.g^{-1}{\cdot}min^{-1}$ (Qiao et al., 2021).

Overall, the kinetic characteristics revealed that zinc adsorption was dominated by pseudo-second order and Elovich kinetic models for both biochars, confirming chemisorption as the primary mechanism. Because of its improved textural properties and functional groups, BCC outperformed BCN in terms of adsorption capacity and rate. Similar findings from literature studies show that pseudo-second order and Elovich kinetic models best describe the zinc adsorption process for various

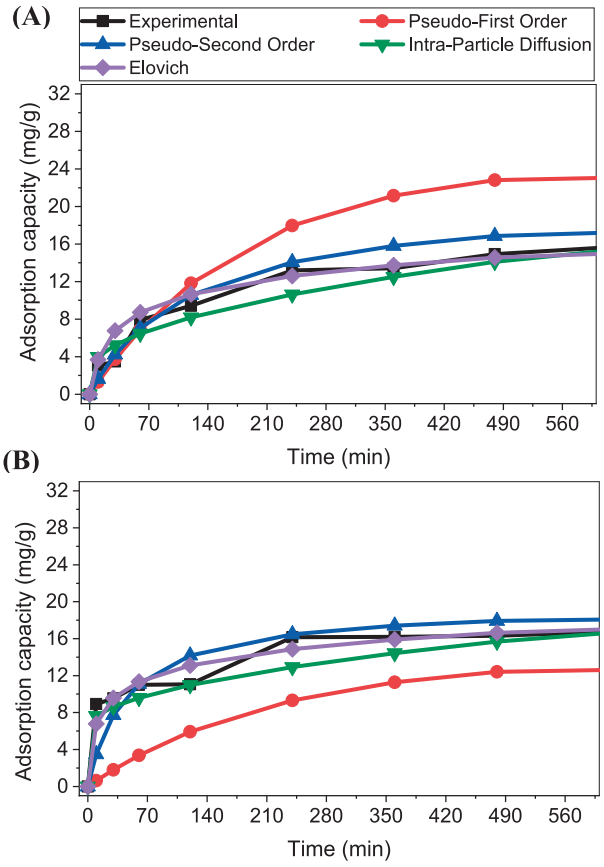

Fig. 4. Adsorption kinetics for lead by BCN (A) and BCC (B) biochars (experimental and theoretical).

Table 3
Calculated kinetic parameters for Zn^{2+} and Pb^{2+} by BCN and BCC biochars using different kinetic models.

Kinetic models	Parameters	BCN (Zn^{2+})	BCC (Zn^{2+})	BCN (Pb^{2+})	BCC (Pb^{2+})
Pseudo-first order	K_1 (min^{-1})	0.0043	0.0042	0.0055	0.0046
	q_e (exp)	22.45	26.16	20.12	19.38
	q_e (mg. g^{-1})	4.50	4.82	24.60	13.94
	R^2	0.87	0.88	0.95	0.97
Pseudo-second order	K_2 (g ($min^{-1}mg^{-1}$))	0.0064	0.0049	0.0004	0.0011
	q_e (exp)	22.45	26.16	20.12	19.38
	q_e ($mg.g^{-1}$)	22.51	26.22	21.03	19.65
	R^2	0.99	0.99	0.99	0.99
Intra-Particle Diffusion	K_{diff} (mg/g. $min^{0.5}$)	0.37	0.38	0.54	0.43
	C	13.23	16.65	2.27	6.27
	R^2	0.28	0.19	0.91	0.71
Elovich	β ($g.mg^{-1}$)	0.35	0.34	0.36	0.39
	α (mg. $g^{-1}{\cdot}min^{-1}$)	22.67	55.18	1.04	3.65
	R^2	0.75	0.71	0.91	0.95

biochars such as carp biochars (Qiao et al., 2021), rice husk, wood chip, and bamboo (Van Hien et al., 2020), corn straw (Chen et al., 2011), and cattle manure (Kołodyńska et al., 2012).

Concerning Pb^{2+} adsorption kinetics, the experimental and theoretical adsorption capacities calculated from various kinetic models are plotted in Fig. 4, and the corresponding parameters are listed in Table 3.

As shown in Fig. 4, for both biochars, the PFO model demonstrated a moderate fit, with R^2 values of 0.95 (BCN) and 0.97 (BCC). The PFO model estimated the equilibrium adsorption capacity for BCN to be 24.60 mg/g compared to the experimental value of 20.12 mg/g, and for BCC, it was 19.38 mg/g compared to the experimental value of 13.94 mg/g. Additionally, the BCN rate constant (K_1) was slightly higher (0.0055) than BCC one (0.0046), indicating a quicker rate of initial adsorption. Consequently, the PFO model provided a moderate fit but was unable to fully describe the adsorption process, especially for later-stage adsorption where diffusion effects predominate (Kołodyńska et al., 2012; Shi et al., 2019).

The PSO kinetic model demonstrated high agreement between theoretical and experimental adsorption data for BCN and BCC, with an R^2 value of 0.99. The calculated adsorption capacity values (20.12 mg/g for BCN and 19.38 mg/g for BCC) were very close to the experimental values (21.03 mg/g and 19.65 mg/g), indicating that the PSO model accurately described Pb^{2+} adsorption (Wang et al., 2022a). Furthermore, BCC had a significantly higher rate constant (K_2) (0.0011) than BCN (0.0004), indicating a faster adsorption rate. Overall, both biochars exhibited PSO kinetics, indicating that chemisorption was the main mechanism. BCC showed higher adsorption, possibly due to its reactive functional groups (Kwak et al., 2019).

The IPD model also provided a moderate fit for both biochars, with R^2 values of 0.91 (BCN) and 0.71 (BCC), suggesting that it may not accurately describe the entire adsorption process. Furthermore, BCN had a higher diffusion rate constant (K_{diff}) (0.54) than BCC (0.43), indicating faster intra-particle diffusion in BCN (Kołodyńska et al., 2012).

In terms of Elovich kinetics, the β (0.36) and α (1.04) values for BCN showed moderate initial adsorption rates that gradually slowed down over time. The R^2 value of 0.91 suggested a reasonable model fit, supporting chemisorption processes. In comparison to BCN, BCC's higher α value (3.65) suggested a much faster initial adsorption, followed by site saturation with an R^2 value of 0.95, indicating a better fit (Largitte and Pasquier, 2016).

Overall, like Zn^{2+} adsorption, Pb^{2+} adsorption was dominated by pseudo-second-order kinetics for both biochars, confirming chemisorption as the primary mechanism, while the IPD and Elovich models further supported the multi-step adsorption process. Literature studies on Pb^{2+} adsorption also reported that PSO was the best fit for different biochars (Wang et al., 2022a), including cattle manure biochars (Kołodyńska et al., 2012), sawdust and wheat straw biochars (Kwak et al., 2019), sugarcane bagasse and orange peel biochars (Abdelhafez and Li, 2016).

3.2.3. Elemental composition of biochar before and after Zn^{2+} and Pb^{2+} adsorption

To gain a better understanding of the adsorption process, elemental (EDS) analyses were performed on both biochars before and after metal adsorption (Zn^{2+} and Pb^{2+}). For each biochar, four different points were examined, and the average weight percentage (wt.%) of each metal is shown in Table 4, the atomic percentages (at.%) and representative EDS spectra are presented in Table S2 Fig. S4 (Supplementary materials).

As shown in Table 4, BCC had slightly higher C and Si, while P content was lower than BCN because of the CO_2 atmosphere during pyrolysis (Premchand et al., 2024a), while no Zn^{2+} and Pb^{2+} were found before adsorption. Following zinc adsorption, the C content of the BCN decreased from 73.5 to 64.4 wt% (81.7 to 75.1 at.% in Table S2), while its O content increased from 15.9 to 21.3 wt% (13.2 to 18.6 at.% in Table S2), implying partly due to mass dilution effect because of the Zn^{2+} uptake and partly due to surface modification caused by metal complexation or precipitation on active carbon and oxygen sites (Qiao et al., 2021). Furthermore, a significant Zn^{2+} concentration (1.82 wt% in Table 4 and 0.4 at.% Table S4) was found in BCN, indicating an effective Zn^{2+} binding (Zhao et al., 2020). BCC, on the other hand, showed a more pronounced trend of decreasing C and increasing O contents. Moreover, BCC had a significantly higher Zn^{2+} concentration (6.3 wt% in Table 4 and 1.6 at. % in Table S4) than BCN, which is consistent with BCC's higher Zn^{2+} adsorption efficiency and can be correlated with its improved porosity, oxygen functionalities, and specific surface area, as previously discussed.

Examining the Pb^{2+} adsorption, the C content of the BCN decreased slightly from 73.5 to 72.9 wt% (81.7 to 82.7 at.% in Table S4), whereas the O content increased slightly from 15.9 to 16.5 wt% (13.3 to 14.0 at. % in Table S4), indicating limited structural modifications or a modest participation of oxygen functional group in Pb^{2+} binding (Chi et al., 2017). Furthermore, a large amount of Pb^{2+} was found (3.6 wt% and 0.2 at.%), indicating high Pb^{2+} adsorption effectiveness. On the other hand, the C content of the BCC decreased while the O content increased more dramatically than in the BCN, indicating extensive Pb^{2+} interaction on carbon surfaces and the role of oxygen functionalities in Pb^{2+} adsorption (Qiao et al., 2021). Furthermore, a slightly lower Pb^{2+} content (2.1 wt% and 0.2 at. %) was observed in BCC, corroborating prior findings of BCC having a slightly lower Pb^{2+} adsorption capability than BCN.

From the mechanistic point of view, based on current data and literature studies, adsorption behavior appears synergistic with a combination of several mechanisms, including ion-exchange, surface complexation, and electrostatic interaction.

3.3. Biochar-soil incubation studies

3.3.1. Effect of biochar application on physicochemical properties of soil

The effect of different doses of biochar amendments on CHNS analysis of soil is given in Table 5.

The total carbon content of the control soil was 7.46 %. Following the addition of biochars, the carbon content of the soil increased in direct proportion to the biochar doses (3 %, 5 %, and 10 %, respectively). In general, biochar's higher carbon content causes soil carbon enrichment (Jin et al., 2016). BCN amendment increased soil carbon content from 7.46 % to 9.78 %, 11.24 %, and 13.22 % at 3 %, 5 %, and 10 % doses, respectively, whereas BCC amendment increased soil carbon content to 9.77 %, 10.77 %, and 13.95 % at similar doses. The statistical analysis revealed a significant effect of biochar dose on total carbons ($p < 0.0001$), while there was no statistical difference between biochar types ($p > 0.05$). A post-hoc test revealed that the three doses of biochar (3 %, 5 %, and 10 %) differed from each other ($p < 0.05$), confirming that total carbon increased significantly with increasing biochar dose, with 10 % being the highest, regardless of biochar type. Similarly, both biochars also increased the soil hydrogen contents from 1.32 % to 1.54 % and nitrogen contents from 0.62 % to 0.73 % (BCN) and from 0.62 %

Table 4
Elemental composition (weight %) of biochars (BCN and BCC) before and after Zn^{2+} and Pb^{2+} adsorption (values are reported as a mean ± standard deviation; n = 3).

	C	O	Si	Mg	K	Ca	Zn	Pb
BCN	73.5 ± 2.5	15.9 ± 2.3	9.9 ± 0.3	N/D	0.63 ± 0.23	0.13 ± 0.02	N/D	N/D
BCC	75.2 ± 3.8	13.2 ± 2.8	10.6 ± 1.1	0.14 ± 0.05	0.63 ± 0.13	0.19 ± 0.08	N/D	N/D
BCN (Zn^{2+})	64.4 ± 9.5	21.3 ± 5.5	10.8 ± 4.1	0.13 ± 0.08	0.77 ± 0.20	0.37 ± 0.09	1.8 ± 1.2	N/D
BCC (Zn^{2+})	53.0 ± 2.5	16.5 ± 6.6	13.5 ± 2.4	2.00 ± 1.51	2.49 ± 0.69	1.69 ± 0.23	6.3 ± 1.2	N/D
BCN (Pb^{2+})	72.9 ± 4.8	16.5 ± 4.4	5.4 ± 2.2	0.18 ± 0.03	0.54 ± 0.22	0.25 ± 0.07	N/D	3.6 ± 1.4
BCC (Pb^{2+})	57.7 ± 10.4	23.1 ± 7.3	15.7 ± 4.3	0.06 ± 0.06	0.61 ± 0.44	0.26 ± 0.27	N/D	2.1 ± 0.7

N/D - not detected.

Table 5
Effect of biochar's application on elemental analysis of soil (3, 5, and 10 represent the biochar doses of 3, 5, and 10 %, and different alphabets represent the significant difference between biochar type and dosage at $p < 0.05$).

Sample	C (%)	H (%)	N (%)	S (%)	C/N	C/H
CS	7.46 ± 0.11	1.32 ± 0.02	0.62 ± 0.01	1.20 ± 0.05	12.03	5.65
3-BCN	9.78 ± 0.64c	1.48 ± 0.10	0.68 ± 0.03	1.16 ± 0.09	14.38	6.61
3-BCC	9.77 ± 0.15c	1.45 ± 0.03	0.69 ± 0.03	0.97 ± 0.16	14.16	6.74
5-BCN	11.24 ± 0.74b	1.51 ± 0.05	0.73 ± 0.03	1.12 ± 0.13	15.40	7.44
5-BCC	10.77 ± 0.43b	1.51 ± 0.02	0.71 ± 0.02	1.20 ± 0.30	15.17	7.13
10-BCN	13.22 ± 1.33a	1.54 ± 0.05	0.73 ± 0.04	1.10 ± 0.16	18.11	8.58
10-BCC	13.95 ± 1.25a	1.54 ± 0.13	0.76 ± 0.05	0.95 ± 0.26	18.36	9.06

to 0.76 % (BCC) with a higher biochar dose of 10 %, with BCC being greater than BCN.

Overall, because the biochars contained high levels of C and N, they considerably increased the soil C and N content through direct input. Biochar has been considered to increase soil organic carbon and adjust the nitrogen cycle, and it can retain soil nitrogen for years due to its increased porosity and surface area (Clough et al., 2013; Cui Yue Feng et al., 2017). Similar findings have been reported for various biochars and soils, including manure biochar (silt loam and clay loam soils) (Jin et al., 2016), giant reed biochar (silt loam soil) (Zheng et al., 2013), and wood biochar (highly weathered soil) (Jien and Wang, 2013).

Furthermore, the effect of biochar amendment on soil pH, EC, CEC, WHC, carbonates, and organic carbons is depicted in Fig. 5.

The pH of the control soil was 6.79, which was increased to 6.92, 7.12, and 6.95 by adding 3 %, 5 %, and 10 % BCN, respectively, whereas BCC increased the soil pH to 6.95, 7.32, and 7.02 at similar biochar doses. Statistically, biochar type showed significant differences at only 5 % biochar dose, with BCC having a higher pH than BCN, while there were no differences between the 3 % and 10 % biochar types, indicating a nonlinear dose–response. Biochar has been reported to have varying effects on soil pH and is highly dependent on soil type. In general, it significantly increases the pH of acidic soil while having a minor effect on neutral to alkaline pH soil (Jien and Wang, 2013; Zhang et al., 2021). In the current study, both biochars, BCN with a pH of 8.84 and BCC with a pH of 9.57, increased the maximum soil pH at the 5 % dose, due to the liming potential of alkaline biochars (Jien and Wang, 2013). At a higher dose of 10 %, both biochars slightly reduced pH compared to lower doses, possibly because too much biochar oversaturated the soil with carbonates and alkaline components, reducing buffering effectiveness (Liu et al., 2018b). Examining the electrical conductivity (EC), as depicted in Fig. 5(b), biochar dose significantly increased ($p < 0.05$) the EC of the soil only at higher dose (10 %), while no significant differences were observed between the two biochars at all doses. The increase in EC at higher biochar dose was possibly due to the addition of ashes and carbonates present in biochars.

Furthermore, the addition of both biochars significantly ($p < 0.05$) increased the soil WHC, which was directly proportional to the dose applied. BCN increased soil WHC by 262 %, while BCC increased it by 285 %. The WHC is directly related to the textural properties of the biochar; biochar with a large specific surface area and pore volume tends to hold more water and vice versa (de Sousa Lima et al., 2018; Mao et al., 2019). BCC had a higher WHC enhancement than BCN due to its larger specific surface area and porosity. On the other hand, the CEC of control soil was 22.6 meq/100 g, which was raised by 13.4 % by BCN and 9.8 % by BCC at a higher dose of 10 %. These differences, however, were not statistically significant ($p > 0.05$), indicating that the application of biochar may numerically increase CEC. The improvement of CEC through biochar application has been widely reported in the literature (Jien and Wang, 2013; Jin et al., 2016). Generally, biochar improves soil CEC because of its negatively charged functional groups, high surface area, and influence on soil pH (Liu et al., 2018b; Zhang et al., 2021). Despite having a higher specific area, pH, and ash contents than BCN, BCC increased soil CEC slightly less than BCN, which could be attributed to BCC lower O/C ratio (0.30) than BCN (0.34) because CEC value is proportional to O/C value of biochar, i.e., the higher the O/C value, more oxygen-functional groups, and higher the CEC (Lee et al., 2010).

Finally investigating the effect of biochar application on soil organic carbons (SOC), as shown in Fig. 5(F), both biochars significantly ($p < 0.05$) increased the SOC in proportion to the biochar dose, similar to the effect on total C content. Nonetheless, no significant difference was found between the two biochars at any dose, implying that the biochar dose primarily increased the SOC, not the pyrolysis atmosphere. The addition of biochar to soil can increase its SOC in a variety of ways, including direct carbon input, soil microbial activity, and organic matter retention. Since biochar contains highly stable carbon structures that are resistant to both biotic and abiotic degradation, its application results in an increase in soil organic carbon (Singh et al., 2022; Zhang et al., 2021).

3.3.2. *Effect of biochar on bioavailability of PTE in soil*

The effect of both biochars on the bioavailability of PTE in the soil after 5 weeks of incubation is presented in Table 6.

The control soil contained a higher available concentration of zinc (858 mg/kg), followed by manganese (Mn) with 101.3 mg/kg, cadmium (Cd) with 23.8 mg/kg, nickel (Ni) with 1.25 mg/kg, copper (Cu) with 1.13 mg/kg, lead (Pb) with 0.24 mg/kg, and chromium (Cr) with 0.15 mg/kg, respectively. Overall, the addition of both biochars resulted in a consistent trend of a numerical reduction in bioavailable PTE concentrations compared to the control soil and the declines were more pronounced at higher biochar doses, suggesting a dose-dependent trend. For example, BCN reduced Zn^{2+} availability in soil by 7.1 %, 4.2 %, and 5.0 % at 3 %, 5 %, and 10 % biochar doses, whereas the BCC reduced Zn^{2+} availability by 7.8 %, 10.4 %, and 6.0 % at 3 %, 5 %, and 10 % biochar doses, respectively and same trend of numerical reduction was observed for all other metals.

However, it is worth noting that the statistical analyses revealed no significant differences ($p > 0.05$) between the control and treated soils, nor between different types or doses of biochar. Consequently, the current study does not provide direct evidence of effective PTE immobilization by both tested biochars, and numerical reductions in PTE bioavailability can only be used to generate hypotheses for future studies, such as longer biochar-soil incubation time, larger sample size, and robust statistical analyses.

Despite of the effective performance in adsorbing aqueous metals, improving soil's properties, the applications of biochars in the soil did not significantly alter the bioavailability of PTEs and that could be attributed to several possible reasons because the effect depends on many factors, such as biochar feedstock type, processing conditions, type of soil and its properties, sample size as well as incubation time (Medyńska-Juraszek and Ćwieląg-Piasecka, 2020). In many soils (particularly mineral or clay-rich), metals are already strongly bound/adsorbed on their surfaces, and biochar cannot compete due to their strong affinities towards minerals/clays. For example, (Shen et al., 2016) did not find the immobilization of Pb^{2+} in the kaolin-rich soil by the application of hardwood biochar for 28 days, possibly due to the high affinity of Pb^{2+} toward kaolin itself. Another possible explanation is the buffering effect, as metal adsorption is highly pH dependent, and biochar performs better in acidic soils than in neutral/alkaline soils because adding biochar does not significantly change the pH of the soil (a slight increase), effectively stopping the adsorption mechanism (Zhang et al., 2021). In a study on the effects of biochar (wheat straw) on the immobilization of various metals in acidic and neutral to alkaline soil, (Medyńska-Juraszek and Ćwieląg-Piasecka, 2020) discovered that

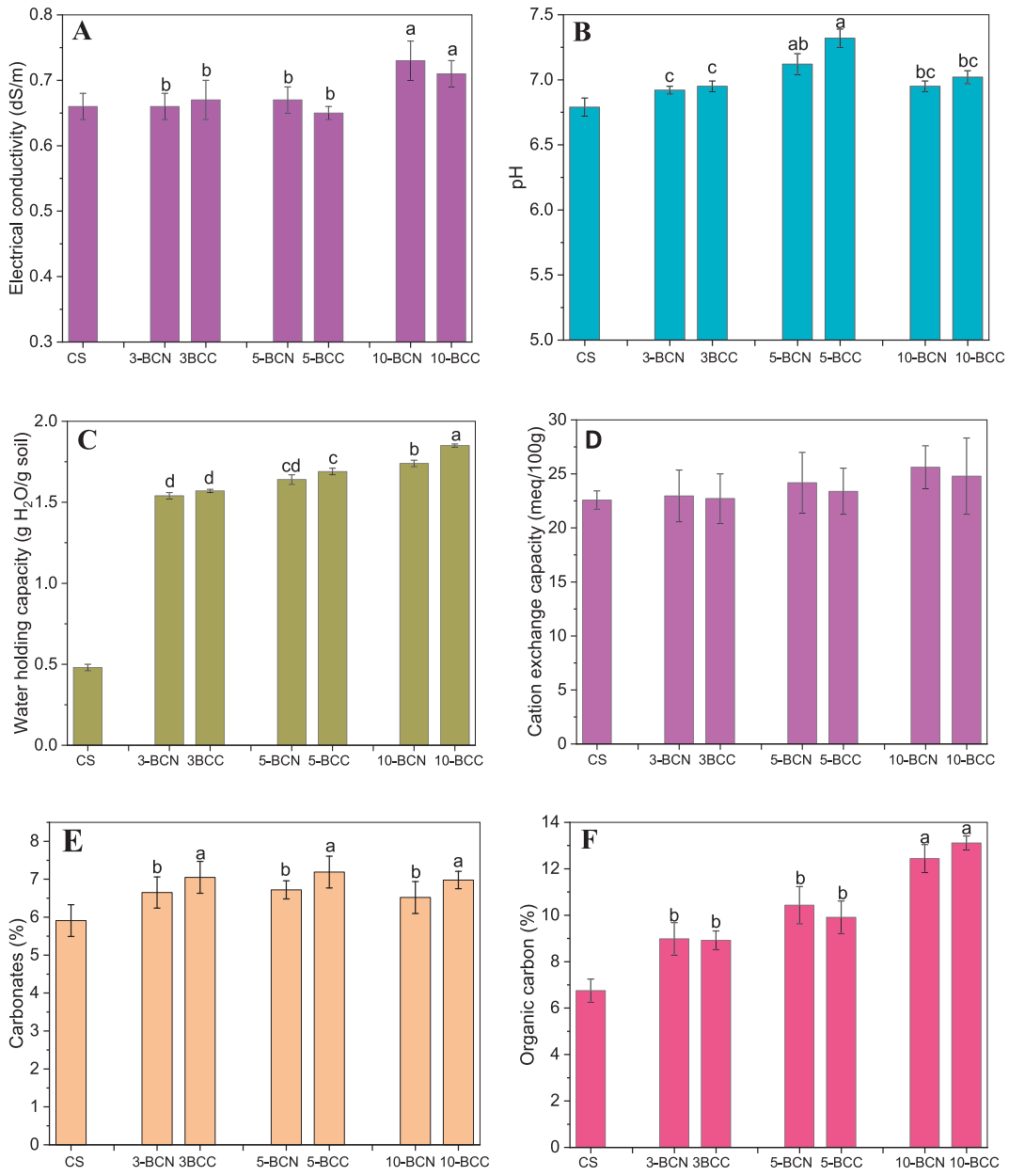

Fig. 5. Effect of biochar application on soil electrical conductivity (EC, dS/m) (A), pH (−) (B), water holding capacity (WHC, g H_2O/g soil) (C), cation exchange capacity (CEC, meq/100 g) (D), carbonates (%) (E), and organic carbon (F). Different letters (a,b) represent the significant difference between biochar type and dosage at $p < 0.05$).

while biochar had no effect on neutral to alkaline soil, it significantly decreased the bioavailability of the various metals in acidic soil which could be directly related to the current study as the pH of the tested soils in the both studies are quite similar (6.8 and 6.4, respectively).

Other possible reasons might be due to the pore blocking of biochar in the soil, or the complex formation of organic matter and metals in the soil.

4. Limitations and recommendations

The current study aimed to assess the short-term performance of CO_2 modified biochar in the remediation of water and soil in comparison to typical N_2 biochar. The findings suggested that 5 weeks incubation were insufficient for the long-term performance assessment in the soil. Further incubation trials with larger sample sizes and longer durations are required in the future to investigate the effect of biochars on soil remediation. Furthermore, since the tested soil in the current study was neutral, which might have hindered the immobilization of PTE's due to the liming effect, future studies should also focus on different soil types, specifically acidic soils. Finally, due to the lack of detailed chemical analyses of the tested biochars, it was not possible to draw an exact mechanism of adsorption and immobilization; therefore, future research should focus on detailed analysis of biochars before and after adsorption.

5. Conclusions

In this study, rice husk biochars produced through pyrolysis in N_2 (BCN) and CO_2 atmospheres (BCC) were evaluated for their efficacies in removing aqueous heavy metals (Zn^{2+} and Pb^{2+}), improving the physicochemical properties of mining contaminated soil, and immobilizing potentially toxic elements (PTE) in the soil through short-term biochar-

Table 6
Bioavailable (DTPA extractable) metals content in the treated soils (values are reported as a mean ± standard deviation; n = 3).

Sample	Cd (mg/kg)	Cr (mg/kg)	Cu (mg/kg)	Mn (mg/kg)	Ni (mg/kg)	Pb (mg/kg)	Zn (mg/kg)
CS	23.8 ± 3.5	0.15 ± 0.01	1.13 ± 0.17	101.3 ± 3.3	1.25 ± 0.24	0.24 ± 0.01	858 ± 91
3-BCN	23.1 ± 4.0	0.14 ± 0.01	1.10 ± 0.19	78.8 ± 22.6	1.25 ± 0.16	0.16 ± 0.01	798 ± 88
3-BCC	19.5 ± 0.8	0.14 ± 0.01	0.98 ± 0.07	77.8 ± 3.5	1.11 ± 0.03	0.14 ± 0.01	791 ± 31
5-BCN	20.5 ± 3.5	0.14 ± 0.01	1.12 ± 0.10	96.4 ± 22.3	1.31 ± 0.08	0.21 ± 0.01	822 ± 11
5-BCC	20.4 ± 1.1	0.14 ± 0.01	0.92 ± 0.13	75.9 ± 13.4	1.12 ± 0.02	0.18 ± 0.01	769 ± 24
10-BCN	23.2 ± 2.5	0.14 ± 0.01	1.12 ± 0.06	94.5 ± 17.5	1.30 ± 0.13	0.18 ± 0.01	808 ± 42
10-BCC	20.3 ± 0.7	0.14 ± 0.01	0.97 ± 0.05	88.8 ± 23.2	1.11 ± 0.01	0.18 ± 0.01	806 ± 19

soil incubation studies. The findings revealed that aqueous Zn^{2+} and Pb^{2+} removal was dominated by pseudo-second-order kinetics for both biochars, confirming chemisorption as the primary mechanism, with BCC having higher Zn^{2+} capacity and adsorption rate than BCN, while for Pb^{2+}, BCC showed higher adsorption in the early stage and eventually became comparable to BCN until 24 h. Moreover, the effect of biochar amendments on soil physicochemical properties indicated that both biochars increased total carbon, organic carbon, nitrogen contents, and water holding capacity in proportion to the applied dose; however, no significant differences were observed among the two biochars despite having statistically different physicochemical properties. Furthermore, both biochars numerically reduced the bioavailability of various PTE (Zn, Cr, Cu, Pb, Mn, Cd, and Ni) in the soil; however, no statistical difference was found between the control soil and various biochar-amended soils, which require further in-depth future studies. Overall, this study emphasized the utilization of waste or recycled CO_2 from industrial flue gases or within pyrolysis systems to produce biochar with an improved textural property through economic (cost saving of inert gas) and environmental (utilizing problematic waste gas) platforms.

CRediT authorship contribution statement

Premchand Premchand: Writing – original draft, Investigation, Formal analysis, Data curation. **Francesca Demichelis:** Writing – original draft, Visualization, Supervision, Methodology, Data curation, Conceptualization. **Elio Padoan:** Methodology, Conceptualization. **Faten Khelifi:** Data curation. **David Chiaramonti:** Validation, Supervision. **Samir Bensaid:** Validation, Supervision. **Debora Fino:** Supervision, Project administration, Funding acquisition.

Declaration of competing interest

The authors declare that they have no known competing financial interests or personal relationships that could have appeared to influence the work reported in this paper.

Acknowledgment

This article and associated research were conducted as part of the Italian inter-university PhD program in sustainable development and climate change (https://www.phd-sdc.it/).

Appendix A. Supplementary data

Supplementary data to this article can be found online at https://doi.org/10.1016/j.ces.2026.123315.

Data availability

Data will be made available on request.

References

Abdelhafez, A.A., Li, J., 2016. Removal of Pb (II) from aqueous solution by using biochars derived from sugar cane bagasse and orange peel. J. Taiwan Inst. Chem. Eng. 61, 367–375. https://doi.org/10.1016/j.jtice.2016.01.005.

Aktar, S., Hossain, M.A., Rathnayake, N., Patel, S., Gasco, G., Mendez, A., de Figueiredo, C., Surapaneni, A., Shah, K., Paz-Ferreiro, J., 2022. Effects of temperature and carrier gas on physico-chemical properties of biochar derived from biosolids. J. Anal. Appl. Pyrol. 164, 105542. https://doi.org/10.1016/j.jaap.2022.105542.

Alam, M.S., Gorman-Lewis, D., Chen, N., Flynn, S.L., Ok, Y.S., Konhauser, K.O., Alessi, D. S., 2018. Thermodynamic analysis of nickel (II) and zinc (II) adsorption to biochar. Environ. Sci. Technol. 52, 6246–6255. https://doi.org/10.1021/acs.est.7b06261.

Asgari, G., Abdipour, H., 2025. Ecological risk assessment and distribution of heavy metals (Pb, Cr, Ni, as, Co and Mn) in soil of Douroud city, Iran. Soil and Sediment Contamination: an International Journal, pp. 1-18. 10.22059/imj.2025.400868.1008263.

Chen, X., Chen, G., Chen, L., Chen, Y., Lehmann, J., McBride, M.B., Hay, A.G., 2011. Adsorption of copper and zinc by biochars produced from pyrolysis of hardwood and corn straw in aqueous solution. Bioresour. Technol. 102, 8877–8884. https://doi.org/10.1016/j.biortech.2011.06.078.

Chi, T., Zuo, J., Liu, F., 2017. Performance and mechanism for cadmium and lead adsorption from water and soil by corn straw biochar. Front. Environ. Sci. Eng. 11, 1–8. https://doi.org/10.1007/s11783-017-0921-y.

Cho, D.-W., Kwon, E.E., Kwon, G., Zhang, S., Lee, S.-R., Song, H., 2017. Co-pyrolysis of paper mill sludge and spend coffee ground using CO2 as reaction medium. J. CO2 Util. 21, 572–579. https://doi.org/10.1016/j.jcou.2017.09.003.

Cho, D.-W., Kwon, E.E., Song, H., 2016. Use of carbon dioxide as a reaction medium in the thermo-chemical process for the enhanced generation of syngas and tuning adsorption ability of biochar. Energ. Conver. Manage. 117, 106–114. https://doi.org/10.1016/j.enconman.2016.03.027.

Clough, T.J., Condron, L.M., Kammann, C., Müller, C., 2013. A review of biochar and soil nitrogen dynamics. Agronomy 3, 275–293. https://doi.org/10.3390/agronomy3020275.

Cui Yue Feng, C.Y., Meng Jun, M.J., Wang QingXiang, W.Q., Zhang WeiMing, Z.W., Cheng XiaoYi, C.X., Chen WenFu, C.W., 2017. Effects of straw and biochar addition on soil nitrogen, carbon, and super rice yield in cold waterlogged paddy soils of North China. 10.1016/S2095-3119(16)61578-2.

Dai, J., Becquer, T., Rouiller, J.H., Reversat, G., Bernhard-Reversat, F., Nahmani, J., Lavelle, P., 2004. Heavy metal accumulation by two earthworm species and its relationship to total and DTPA-extractable metals in soils. Soil Biol. Biochem. 36, 91–98. https://doi.org/10.1016/j.soilbio.2003.09.001.

de Sousa Lima, J.R., de Moraes Silva, W., de Medeiros, E.V., Duda, G.P., Corrêa, M.M., Martins Filho, A.P., Clermont-Dauphin, C., Antonino, A.C.D., Hammecker, C., 2018. Effect of biochar on physicochemical properties of a sandy soil and maize growth in a greenhouse experiment. Geoderma 319, 14–23. https://doi.org/10.1016/j.geoderma.2017.12.033.

Fan, J., Zhang, X., He, N., Song, F., Wang, X., 2025. Investigation on novel deep eutectic solvents with high carbon dioxide adsorption performance. J. Environ. Chem. Eng., 117870 https://doi.org/10.1007/s12355-025-01663-6.

Gao, Y., Wu, P., Jeyakumar, P., Bolan, N., Wang, H., Gao, B., Wang, S., Wang, B., 2022. Biochar as a potential strategy for remediation of contaminated mining soils: Mechanisms, applications, and future perspectives. J. Environ. Manage. 313, 114973. https://doi.org/10.1016/j.jenvman.2022.114973.

Jahan, A., Sarkar, M.I.U., Naher, U.A., Biswas, J.C., Islam, A., 2024. Effect of sterile rice spikelets derived biochar amendment on nutrient leaching and availability in paddy soil under continuous standing water. Geol. Ecol. Landscapes 8, 574–582. https://doi.org/10.1080/24749508.2022.2163608.

Jien, S.-H., Wang, C.-S., 2013. Effects of biochar on soil properties and erosion potential in a highly weathered soil. Catena 110, 225–233. https://doi.org/10.1016/j.catena.2013.06.021.

Jin, Y., Liang, X., He, M., Liu, Y., Tian, G., Shi, J., 2016. Manure biochar influence upon soil properties, phosphorus distribution and phosphatase activities: a microcosm incubation study. Chemosphere 142, 128–135. https://doi.org/10.1016/j.chemosphere.2015.07.015.

Kılıç, M., Kırbıyık, Ç., Çepelioğullar, Ö., Pütün, A.E., 2013. Adsorption of heavy metal ions from aqueous solutions by bio-char, a by-product of pyrolysis. Appl. Surf. Sci. 283, 856–862. https://doi.org/10.1016/j.apsusc.2013.07.033.

Kołodyńska, D., Wnętrzak, R., Leahy, J., Hayes, M., Kwapiński, W., Hubicki, Z., 2012. Kinetic and adsorptive characterization of biochar in metal ions removal. Chem. Eng. J. 197, 295–305. https://doi.org/10.1016/j.cej.2012.05.025.

Kumar, S., Masto, R.E., Ram, L.C., Sarkar, P., George, J., Selvi, V.A., 2013. Biochar preparation from Parthenium hysterophorus and its potential use in soil application. Ecol. Eng. 55, 67–72. https://doi.org/10.1016/j.ecoleng.2013.02.011.

Kwak, J.-H., Islam, M.S., Wang, S., Messele, S.A., Naeth, M.A., El-Din, M.G., Chang, S.X., 2019. Biochar properties and lead (II) adsorption capacity depend on feedstock type, pyrolysis temperature, and steam activation. Chemosphere 231, 393–404. https://doi.org/10.1016/j.chemosphere.2019.05.128.

Largitte, L., Pasquier, R., 2016. A review of the kinetics adsorption models and their application to the adsorption of lead by an activated carbon. Chem. Eng. Res. Des. 109, 495–504. https://doi.org/10.1016/j.cherd.2016.02.006.

Lee, J., Yang, X., Cho, S.-H., Kim, J.-K., Lee, S.S., Tsang, D.C., Ok, Y.S., Kwon, E.E., 2017. Pyrolysis process of agricultural waste using CO2 for waste management, energy recovery, and biochar fabrication. Appl. Energy 185, 214–222. https://doi.org/10.1016/j.apenergy.2016.10.092.

Lee, J.W., Kidder, M., Evans, B.R., Paik, S., Buchanan Iii, A., Garten, C.T., Brown, R.C., 2010. Characterization of biochars produced from cornstovers for soil amendment. Environ. Sci. Technol. 44, 7970–7974. https://doi.org/10.1021/es101337x.

Li, B., Wang, X., Khurshid, A., Saleem, S.F., 2025. Environmental governance, green finance, and mitigation technologies: pathways to carbon neutrality in European industrial economies. Int. J. Environ. Sci. Technol. 1–14. https://doi.org/10.1007/s13762-025-06608-w.

Li, B., Wu, H., Liu, X., Zhu, T., Liu, F., Zhao, X., 2020. Simultaneous removal of SO2 and NO using a novel method with red mud as absorbent combined with O3 oxidation. J. Hazard. Mater. 392, 122270. https://doi.org/10.1016/j.jhazmat.2020.122270.

Liu, Q., Zhang, Y., Liu, B., Amonette, J.E., Lin, Z., Liu, G., Ambus, P., Xie, Z., 2018a. How does biochar influence soil N cycle? A meta-analysis. Plant and Soil 426, 211–225. https://doi.org/10.1007/s11104-018-3619-4.

Liu, Z., Zhang, F., Liu, H., Ba, F., Yan, S., Hu, J., 2018b. Pyrolysis/gasification of pine sawdust biomass briquettes under carbon dioxide atmosphere: study on carbon dioxide reduction (utilization) and biochar briquettes physicochemical properties. Bioresour. Technol. 249, 983–991. https://doi.org/10.1016/j.biortech.2017.11.012.

Lu, H., Li, Z., Gasco, G., Mendez, A., Shen, Y., Paz-Ferreiro, J., 2018. Use of magnetic biochars for the immobilization of heavy metals in a multi-contaminated soil. Sci. Total Environ. 622, 892–899. https://doi.org/10.1016/j.scitotenv.2017.12.056.

Mao, J., Zhang, K., Chen, B., 2019. Linking hydrophobicity of biochar to the water repellency and water holding capacity of biochar-amended soil. Environ. Pollut. 253, 779–789. https://doi.org/10.1016/j.envpol.2019.07.051.

Medyńska-Juraszek, A., Ćwieląg-Piasecka, I., 2020. Effect of biochar application on heavy metal mobility in soils impacted by copper smelting processes. Pol. J. Environ. Stud. 29, 1749–1757. https://doi.org/10.15244/pjoes/108928.

Mehta, N., Cipullo, S., Cocerva, T., Coulon, F., Dino, G.A., Ajmone-Marsan, F., Padoan, E., Cox, S.F., Cave, M.R., De Luca, D.A., 2020. Incorporating oral bioaccessibility into human health risk assessment due to potentially toxic elements in extractive waste and contaminated soils from an abandoned mine site. Chemosphere 255, 126927. https://doi.org/10.1016/j.chemosphere.2020.126927.

Mele, M.A., Kumar, R., Dada, T.K., Heydari, A., Antunes, E., 2024. Investigation of gold adsorption by ironbark biochar using response surface methodology and artificial neural network modelling. J. Clean. Prod. 456, 142317. https://doi.org/10.1016/j.jclepro.2024.142317.

Nguyen, D.L.T., Binh, Q.A., Nguyen, X.C., Nguyen, T.T.H., Vo, Q.N., Nguyen, T.D., Tran, T.C.P., Nguyen, T.A.H., Kim, S.Y., Nguyen, T.P., 2021. Metal salt-modified biochars derived from agro-waste for effective congo red dye removal. Environ. Res. 200, 111492. https://doi.org/10.1016/j.envres.2021.111492.

Padoan, E., Hernandez Kath, A., Vahl, L.C., Ajmone-Marsan, F., 2020. Potential release of zinc and cadmium from mine-affected soils under flooding, a mesocosm study. Arch. Environ. Contam. Toxicol. 79, 421–434. https://doi.org/10.1007/s00244-020-00777-0.

Padoan, E., Romè, C., Mehta, N., Dino, G.A., De Luca, D.A., Ajmone-Marsan, F., 2021. Bioaccessibility of metals in soils surrounding two dismissed mining sites in Northern Italy. Int. J. Environ. Sci. Technol. 18, 1349–1360. https://doi.org/10.1007/s13762-020-02938-z.

Penido, E.S., Martins, G.C., Mendes, T.B.M., Melo, L.C.A., do Rosário Guimarães, I., Guilherme, L.R.G., 2019. Combining biochar and sewage sludge for immobilization of heavy metals in mining soils. Ecotoxicol. Environ. Saf. 172, 326–333. https://doi.org/10.1016/j.ecoenv.2019.01.110.

Premchand, P., Demichelis, F., Chiaramonti, D., Bensaid, S., Fino, D., 2023a. Biochar production from slow pyrolysis of biomass under CO2 atmosphere: a review on the effect of CO2 medium on biochar production, characterisation, and environmental applications. J. Environ. Chem. Eng. 11, 110009. https://doi.org/10.1016/j.jece.2023.110009.

Premchand, P., Demichelis, F., Chiaramonti, D., Bensaid, S., Fino, D., 2023b. Study on the effects of carbon dioxide atmosphere on the production of biochar derived from slow pyrolysis of organic agro-urban waste. Waste Manag. 172, 308–319. https://doi.org/10.1016/j.wasman.2023.10.035.

Premchand, P., Demichelis, F., Galletti, C., Chiaramonti, D., Bensaid, S., Antunes, E., Fino, D., 2024a. Enhancing biochar production: a technical analysis of the combined influence of chemical activation (KOH and NaOH) and pyrolysis atmospheres (N2/CO2) on yields and properties of rice husk-derived biochar. J. Environ. Manage. 370, 123034. https://doi.org/10.1016/j.jenvman.2024.123034.

Premchand, P., Fino, D., Demichelis, F., Bensaid, S., Chiaramonti, D., O'Connell, G., Scott, J., Antunes, E., 2024b. Synthesis of metal-free heteroatom (N, P, O, and B) doped biochar catalysts for enhanced catalytic co-pyrolysis of walnut shells and palm oil fatty acid distillate to produce high-quality bio-oil. J. Environ. Chem. Eng. 12, 113630. https://doi.org/10.1016/j.jece.2024.113630.

Premchand, P., Mead, S., Fino, D., Demichelis, F., Bensaid, S., Chiaramonti, D., Antunes, E., 2025. Sustainable valorisation of cigarette butts waste through pyrolysis: an insight into the pyrolytic products and subsequent aqueous heavy metals removal by pyrolytic char. Chem. Eng. Sci. 302, 120906. https://doi.org/10.1016/j.ces.2024.120906.

Qiao, H.-t., Qiao, Y.-s., Luo, X.-h., Zhao, B.-w., Cai, Q.-y., 2021. Qualitative and quantitative adsorption mechanisms of zinc ions from aqueous solutions onto dead carp derived biochar. RSC Adv. 11, 38273–38282. https://doi.org/10.1039/D1RA05636K.

Rhoades, J., 1982. Cation exchange capacity. Methods of soil analysis: Part 2 chemical and microbiological properties 9, 149-157. 10.2134/agronmonogr9.2.2ed.c8.

Shen, Z., McMillan, O., Jin, F., Al-Tabbaa, A., 2016. Salisbury biochar did not affect the mobility or speciation of lead in kaolin in a short-term laboratory study. J. Hazard. Mater. 316, 214–220. https://doi.org/10.1016/j.jhazmat.2016.05.042.

Shi, J., Fan, X., Tsang, D.C., Wang, F., Shen, Z., Hou, D., Alessi, D.S., 2019. Removal of lead by rice husk biochars produced at different temperatures and implications for their environmental utilizations. Chemosphere 235, 825–831. https://doi.org/10.1016/j.chemosphere.2019.06.237.

Singh, H., Northup, B.K., Rice, C.W., Prasad, P.V., 2022. Biochar applications influence soil physical and chemical properties, microbial diversity, and crop productivity: a meta-analysis. Biochar 4, 8. https://doi.org/10.1007/s42773-022-00138-1.

Tamiru, B, Soromessa, T, Warkineh, B, Legese, G, 2024. Modelling selected soil chemical properties using TerrSet and Random Forest: a case of Hangadi watershed, Taylor & Francis, Oromia, Ethiopia, pp. 1-17. 10.1080/24749508.2024.2429842.

Tan, Z., Ye, Z., Zhang, L., Huang, Q., 2018. Application of the 15N tracer method to study the effect of pyrolysis temperature and atmosphere on the distribution of biochar nitrogen in the biomass–biochar-plant system. Sci. Total Environ. 622, 79–87. https://doi.org/10.1016/j.scitotenv.2017.11.341.

Van Hien, N., Valsami-Jones, E., Vinh, N.C., Phu, T.T., Tam, N.T.T., Lynch, I., 2020. Effectiveness of different biochar in aqueous zinc removal: correlation with physicochemical characteristics. Bioresour. Technol. Rep. 11, 100466. https://doi.org/10.1016/j.biteb.2020.100466.

Wang, C., Wang, X., Li, N., Tao, J., Yan, B., Cui, X., Chen, G., 2022a. Adsorption of lead from aqueous solution by biochar: a review. Clean Technol. 4, 629–652. https://doi.org/10.3390/cleantechnol4030039.

Wang, Y.-Y., You, L.-C., Lyu, H.-H., Liu, Y.-X., He, L.-L., Hu, Y.-D., Luo, F.-C., Yang, S.-M., 2022b. Role of biochar–mineral composite amendment on the immobilization of heavy metals for Brassica chinensis from naturally contaminated soil. Environ. Technol. Innovation 28, 102622. https://doi.org/10.1016/j.eti.2022.102622.

Xiong, J., Hu, Q., Wu, J., Jia, Z., Ge, S., Cao, Y., Zhou, J., Wang, Y., Yan, J., Xie, L., 2023. Structurally stable electrospun nanofibrous cellulose acetate/chitosan biocomposite membranes for the removal of chromium ions from the polluted water. Adv. Compos. Hybrid Mater. 6, 99. https://doi.org/10.1007/s42114-023-00680-x.

Yargicoglu, E.N., Sadasivam, B.Y., Reddy, K.R., Spokas, K., 2015. Physical and chemical characterization of waste wood derived biochars. Waste Manag. 36, 256–268. https://doi.org/10.1016/j.wasman.2014.10.029.

Ye, Z., Liu, L., Tan, Z., Zhang, L., Huang, Q., 2020. Effects of pyrolysis conditions on migration and distribution of biochar nitrogen in the soil-plant-atmosphere system. Sci. Total Environ. 723, 138006. https://doi.org/10.1016/j.scitotenv.2020.138006.

Yu, D., Jiang, Q., Zhu, H., Chen, Y., Xu, L., Ma, H., Pu, S., 2025. Electrochemical reduction for chlorinated hydrocarbons contaminated groundwater remediation: mechanisms, challenges, and perspectives. Water Research, 123149, doi:10.1016/j.watres.2025.123149.

Zhang, Y., Wang, J., Feng, Y., 2021. The effects of biochar addition on soil physicochemical properties: a review. Catena 202, 105284. https://doi.org/10.1016/j.catena.2021.105284.

Zhao, M., Dai, Y., Zhang, M., Feng, C., Qin, B., Zhang, W., Zhao, N., Li, Y., Ni, Z., Xu, Z., 2020. Mechanisms of Pb and/or Zn adsorption by different biochars: biochar characteristics, stability, and binding energies. Sci. Total Environ. 717, 136894. https://doi.org/10.1016/j.scitotenv.2020.136894.

Zheng, H., Wang, Z., Deng, X., Herbert, S., Xing, B., 2013. Impacts of adding biochar on nitrogen retention and bioavailability in agricultural soil. Geoderma 206, 32–39. https://doi.org/10.1016/j.geoderma.2013.04.018.

Zhong, R., Lyu, H., Su, X., Yan, X., Teng, Y., Dong, W., Wan, Y., Song, T., Shen, X., 2025. Freeze–thaw–induced regulation of petroleum hydrocarbon adsorption in cold-region soils: role of organic matter dynamics. Water Research, 124495, doi:10.1016/j.watres.2025.124495.